Biosensors and Bioelectronics 145 (2019) 111705

Contents lists available at ScienceDirect

Biosensors and Bioelectronics

journal homepage: www.elsevier.com/locate/bios

Ratiometric fluorescence sensor for organophosphorus pesticide detection based on opposite responses of two fluorescence reagents to MnO_2 nanosheets

Tiantian Yao[a], Anran Liu[a], Yong Liu[b,**], Min Wei[c], Wei Wei[a,*], Songqin Liu[a]

[a] Jiangsu Engineering Laboratory of Smart Carbon-Rich Materials and Device, Jiangsu Province Hi-Tech Key Laboratory for Bio-medical Research, School of Chemistry and Chemical Engineering, Southeast University, Nanjing, 211189, China
[b] College of Chemistry and Chemical Engineering, Henan University, Kaifeng, 475004, PR China
[c] College of Food Science and Technology, Henan University of Technology, Zhengzhou, 450001, China

ARTICLE INFO

Keywords:
MnO_2 nanosheets
Ratiometric fluorescence
Organophosphorus pesticide
Acetylcholinesterase
Scopoletin
Amplex red

ABSTRACT

The detection of organophosphorus pesticides (OPs) has received considerable attention for their great harm to human beings. Herein, a novel ratiometric fluorescence biosensor was constructed for the determination of OPs by using Scopoletin (SC) and Amplex Red (AR) as probe pairs that have opposite responses to MnO_2 nanosheets (MnO_2 NS). MnO_2 NS possess peroxidase-like catalytic activity, which could quench the fluorescence of SC as well as enhance the fluorescence of the non-fluorescent substance AR by oxidation. In the absence of OPs, acetylcholinesterase (AChE) hydrolyzed acetylcholine chloride (ATCh) into choline (TCh) and acetate. TCh led the decomposition of MnO_2 NS to manganese ions (Mn^{2+}), increasing signal of SC and decreasing signal of AR. In the presence of OPs, the activity of AChE was inhibited and the decomposition of MnO_2 NS was hindered, therefore the fluorescence intensity of SC was weak and the fluorescence intensity of AR had an obvious increase. Moreover, under the optimal conditions, the ratio of fluorescence intensity response recorded on the AR/SC increases with increasing the concentration of DDVP. The method has wider linear range of 5.0 pg/mL ~500 ng/mL with a detection limit of 1.6 pg/mL, which is superior to previously reported methods. This strategy has also been applied to a visual observation based on the color change of the solution under UV light.

1. Introduction

As a common pesticide, organophosphorus pesticides (OPs) are widely used in agricultural production. OPs play a huge role in increasing crop yields and controlling pests and diseases (Hua et al., 2014). However, excessive use of OPs causes different levels of residues existing widely in food, water and the environment (Liu et al., 2014; Mishra et al., 2017). OPs could inhibit the activity of acetylcholinesterase (AChE), it seriously affects human health (Kim et al., 2011). Acetylcholinesterase (AChE) is an acetylcholine hydrolase mainly found in the central nervous system of humans and animals. Its basic function is to catalyze the hydrolysis of the neurotransmitter acetylcholine, which leads to the termination of nerve impulse transmission and thus maintains normal physiological function of cholinergic nerve (Dzudzevic Cancar et al., 2016; Aragay et al., 2012). Therefore, reliable method for detecting and monitoring of OPs has become increasingly important owing to its tight relationship to human health.

Over the past decade, various techniques have been explored to monitor OPs, for instance, liquid chromatography (LC) (Wang et al., 2012), gas chromatography (GC) (Lee and Lee, 2011), gas chromatography coupled with mass spectrometry (GC/MS) (Sang et al., 2013), enzyme-linked immunosorbent assay (ELISA) test (Qian et al., 2009) etc. Most of these methods have the disadvantages of time consuming and complex operations. In order to overcome these shortcomings, methods based on inhibition of enzyme activity of OPs detection have attracted attention. Because OPs can be determined more quickly and simply, they have been widely used in fluorescence (Lu et al., 2018; Yan et al., 2017a, 2018; Huang et al., 2018; Cheng et al., 2018; Wu et al., 2017), colorimetric (Ouyang et al., 2018; Liu et al., 2018; Han and Wang, 2019; Yan et al., 2017b), electrochemical (Zhao et al., 2018; Liu et al., 2017; Wang et al., 2018), surface-enhanced Raman (Tan et al., 2017), etc. Among these methods, fluorescence methods were more sensitive and convenient. For example, Lu et al. reported the detection

* Corresponding author.
** Corresponding author.
E-mail addresses: liuyong@henu.edu.cn (Y. Liu), weiw@seu.edu.cn (W. Wei).

https://doi.org/10.1016/j.bios.2019.111705
Received 13 May 2019; Received in revised form 16 August 2019; Accepted 13 September 2019
Available online 17 September 2019
0956-5663/

of OPs with a Luminescent Dinuclear Ir(III) Complex (Lu et al., 2018), while Yan et al. investigated the fluorescence analysis of OPs based on MnO_2 nanosheet-carbon dots systems (Yan et al., 2018). However, most fluorescent assays are focused on either turn-off or turn-on fluorescence for detection, a single response signal was disturbed by various experimental factors. Ratiometric fluorescent can not only improve the accuracy of measurements but also greatly alleviate external interference (Yang et al., 2017; Wang et al., 2016; Liu et al., 2013). Therefore, a simple, ratiometric fluorescent sensor for sensitive detection of OPs is more precise.

As an excellent 2D nanomaterial, MnO_2 nanosheets have attracted extensive attention in bioanalysis owing to their appealing physicochemical properties (Chen et al., 2015). Firstly, MnO_2 nanosheets have a very broad UV absorption spectrum, which results in a good fluorescence quenching property (Zhao et al., 2014; Yan et al., 2016). Yan et al. developed a turn-on fluorescence OPs detection method based MnO_2 nanosheet-carbon dots systems (Yan et al., 2018). Secondly, according to the unique reaction (ATCh + AChE = HAc + TCh), TCh has the ability to reduce MnO_2 nanosheets to Mn^{2+} (Chen et al., 2014). when OPs were introduced to AChE/MnO_2 nanosheet systems, the decomposition of MnO_2 NS were prevented. Thirdly, MnO_2 nanosheets have the properties of oxidase. Yan et al. explored the strategy for the detection of OPs based on MnO_2 nanosheets catalysis of 3,3′,5,5′tetramethylbenzidine (TMB) (Yan et al., 2017b). As peroxidase substrates (Li et al., 2012), Scopoletin(SC) and Amplex Red(AR) have opposite fluorescence responses to MnO_2 nanosheets (Fan et al., 2017).

Inspired by the aforementioned works, we firstly developed a ratiometric fluorescent biosensor for OPs determination based on the inhibition of enzymatic etching of MnO_2 NS and opposite responses of two fluorogenic substrates to MnO_2 NS. AChE is capable of catalyzing the production of TCh from the substrate ATCh, reducing MnO_2 NS to Mn^{2+}. OPs inhibited the activity of AChE and prevented the production of TCh, thereby there were no decomposition of MnO_2 NS. MnO_2 NS worked as recognizer, giving rise to the change of FL intensity towards SC and AR. Along with fluorescence “Off” and “On” of the two signal molecules caused by OPs, it was the successful ratiometric fluorescence based on MnO_2 NS for the detection of OPs.

2. Experiments

2.1. Materials and reagents

Tetramethylammonium hydroxide and manganese chloride ($MnCl_2$) were obtained from Sinopharm Chemical Reagent Company (Shanghai, China). Scopoletin (SC) (98%) was provided by J&K (Beijing, China). Amplex Red (AR) (≥98%) and hydrogen peroxide (H_2O_2) was purchased from Aladdin Industrial Corporation (Shanghai, China). AChE (Acetylcholinesterase from *Electrophorus electricus* (electric eel)) and ATCh were purchased from Sigma-Aldrich (Shanghai, China). Standards for organophosphorus pesticides such as dichlorvos were purchased from the National Standards Center (Beijing, China). Other reagents were of analytical grade and used directly. The buffer solutions involved in this study were employed as follows:

PB buffer: 25 mM NaH_2PO_4, pH 5; PBS buffer: 137 mM NaCl, 10 mM NaH_2PO_4, 2.7 mM KCl,2 mM KH_2PO_4, pH 8.5; Tris-HCl buffer: 20 mM Tris, pH 7.5. Adjusting buffer solutions with different pH values by hydrochloric acid or sodium hydroxide.

2.2. Instrumentation

The UV–vis spectra and fluorescence spectra were collected by UV–vis spectrophotometer (Cary 100, Agilent, Singapore) and fluorescence spectrometer (FluoroMax-4, HORIBA Jobin Yvon, Japan), separately. The transmission electron microscopy (TEM) equipment (JEM-2100) was from Hitachi, Japan. Dynamic light scattering (DLS) particle sizing and zeta potential measurements were collected using a laser particle analyzer (NanoBrook Omni) from Brookhaven, USA. Visual detection was operated under an UV lamp (ZF-7A, 16 W).The ultrapure water used (18.2 MΩ cm) was taken from the Barnstead ultrapure water system from Thermo Scientific, USA.

2.3. Synthesis of MnO_2 nanosheets

As is reported in previous study, the simple synthesis of MnO_2 nanosheets was performed (Fan et al., 2015). In brief,10 mL of $MnCl_2$ (0.3 M) was quickly added into the mixture containing 20 mL of H_2O_2 (3%) and 0.6 M tetramethylammonium hydroxide within 15 s, and the color of the solution quickly became dark brown and the mixture was stirred for 12 h at room temperature. The reaction mixture was centrifuged at 2000 rpm for 20 min and washed thoroughly with ultrapure water and methanol. Then, the bulk manganese dioxide was dried at 60 °C for the following experiments. To prepare the MnO_2 nanosheets, dispersion was carried out by sonicating the MnO_2 nanosheets solution (1 mg/mL) for 10 h. Then the mixture was centrifuged at 2000 rpm for 30 min, and the supernatant was stored in a refrigerator at 4 °C for further use.

2.4. Decomposition of MnO_2 nanosheets induced by acetylcholinesterase and the fluorescence change of SC and AR

In brief, various concentrations of AChE (50 μL) and 5 mM of ATCh (20 μL) blended with 30 μL of PBS buffer. After the reaction mixture incubated at 37 °C for 30 min, 30 μL of MnO_2 nanosheets solution (0.5 mg/mL) and 54 μL of PB buffer were added. The resultant mixture was incubated for 30 min at room temperature. Next, 6 μL of SC (50 μM) and 10 μL of AR (50 μM) were added to the above mixture and ensure the final volume of 200 μL. The fluorescence spectra of different samples were recorded at room temperature.

2.5. Detection procedures for OPs sensing

First of all, 50 μL mixture containing 40 μL of AChE (0.25 U/mL) and 10 μL of various concentrations of OPs solution were incubated for 30 min at 37 °C. Next, 20 μL of ATCh solution (5 mM) and 30 μL PBS buffer solution were added to the above solution for another 30 min at 37 °C. Then, 30 μL of MnO_2 nanosheets solution (0.5 mg/mL) and 54 μL of PB buffer solution were added and incubated for 30 min at room temperature. Finally, 6 μL of SC (50 μM) and 10 μL of AR (50 μM) were added to the above mixture and reacted in the dark environment for 30 min. Fluorescence spectra were recorded at room temperature. The total volume was 200 μL.

2.6. Detection procedures for OPs sensing in real sample

The collected water from Jiulonghu Lake was centrifuged at 13000 rpm for 30 min in order to remove the insoluble matters. Subsequently, it was filtered by using a 0.22-μm nitrocellulose membrane filter. Then, the water samples were spiked with known concentrations of OPs for further assay experiments.

3. Results and discussion

3.1. Principle of fluorescence sensing strategy

MnO_2 nanosheets, possessing oxidase-like catalytic ability, were prepared beforehand. Scopoletin (SC) and Amplex Red (AR) are the fluorescent substrates of peroxidase and have different responses to MnO_2 NS. As displayed in Fig. 1A, in the absence of MnO_2 nanosheets, SC had a high FL signal at 465 nm (curve a). In the presence of MnO_2 NS, there was a distinct decrease of FL intensity (curve b). As shown in Fig. 1B, AR had no FL signal (curve a) and a high fluorescence signal at 585 nm when MnO_2 NS were added (curve b). When MnO_2 NS were

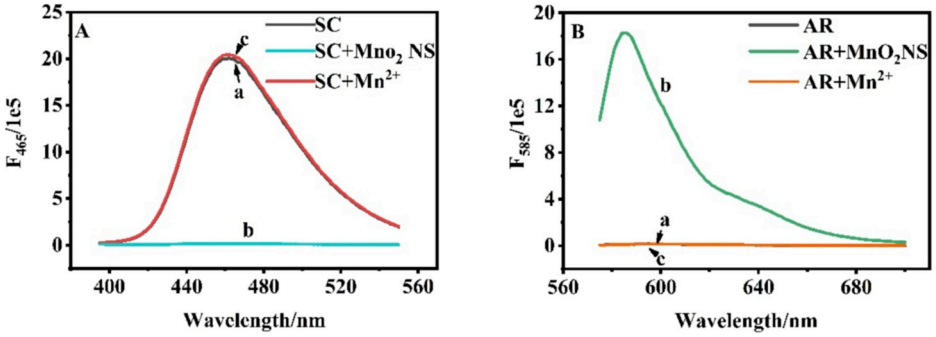

Fig. 1. (A) Fluorescence spectra of SC (a), SC/MnO2 NS (b) and SC/Mn2+ (c). (B) Fluorescence spectra of AR (a), AR/MnO2 NS (b) and AR/Mn2+ (c).

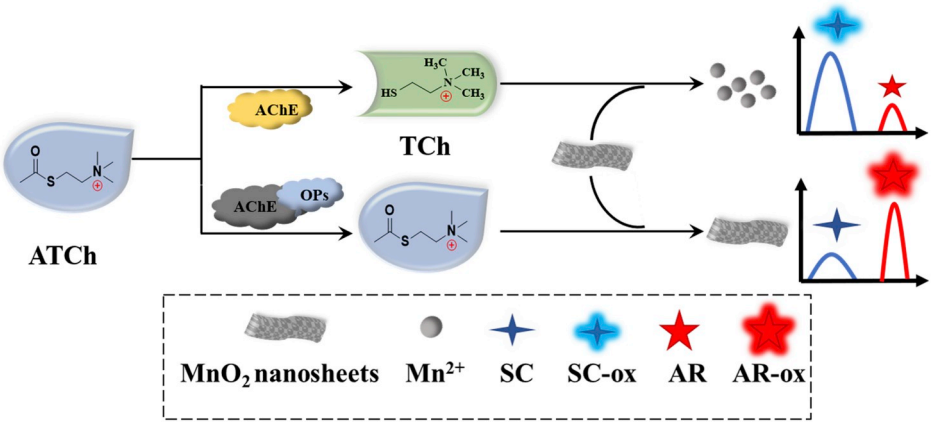

Scheme 1. Schematic description of ratiometric fluorescent sensor for sensitive detection of organophosphorus pesticides based on opposite responses of SC and AR to MnO_2 NS.

replaced with Mn^{2+}, the fluorescence of SC decreased sharply (curve c in Fig. 1A) while it increased sharply for AR (curve c in Fig. 1B).

Principle of ratiometric fluorescent biosensor for organophosphorus pesticides determination was presented in Scheme 1. In the absence of OPs, ATCh were hydrolyzed to produce TCh, etching MnO_2 NS via reduction reaction. As shown in equation (1), MnO_2 NS were reduced to Mn^{2+}. Owing to the destruction of MnO_2 NS, an increase fluorescence intensity of SC and a decrease fluorescence intensity of AR fluorescence were obtained. In the presence of OPs, the activity of AChE was inhibited and no MnO_2 NS were reduced, resulted in a weak FL signal at 465 nm (SC) and a high FL signal at 585 nm (AR). Therefore, by adopting this ratiometric fluorescent approach, highly sensitive determination of OPs can be realized by monitoring the fluorescence signal change of the reaction system. The probe presented a high signal/noise ratio.

which decomposed MnO_2 NS into Mn^{2+}, companying with an increase FL intensity of SC (Fig. 2A(c)) and a decrease FL intensity of AR (Fig. 2B (c)). In the presence of OPs, the enzyme catalytic activity of AChE was inhibited. The oxidation still consisted in the system, therefore the FL intensity of SC was quenched (Fig. 2A(d)) and the FL intensity of AR was enhanced by MnO_2 NS (Fig. 2B(d)). The corresponding solution showed different color under UV light irradiation (insert of Fig. 2).

Furthermore, UV–vis spectrum and Zeta potential were performed to illustrate the decomposition of MnO_2 NS. As shown in Fig. 2C, there was a high UV absorption peak at 360 nm with only ATCh, while a low UV absorption peak with both ATCh and AChE. The insert picture also illustrated the decomposition of MnO_2 NS with obvious color change. As shown in Fig. 2D, the as prepared MnO_2 NS had a negative zeta potential (−25.82 mV, column a). The zeta-potential value of the ATCh/MnO_2 NS/SC/AR system was switched from −27.87 mV

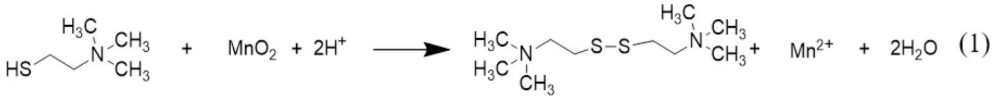

(column b) to −12.65 mV after the AChE added (column c). Inspired from the above results, a ratiometric fluorescent sensor for sensitive detection of OPs was established based on the MnO_2 NS catalyzing the oxidation reaction of SC and AR.

3.2. Feasibility of fluorescence sensing strategy

Feasibility of the strategy for OPs detection was evaluated in this section. When only ATCh existed in the system, because of the oxidation between SC and MnO_2 NS, there were a low FL signal at 465 nm (SC, Fig. 2A(a)) and a high FL signal at 585 nm (AR, Fig. 2B(a)). The FL spectrum of ATCh/MnO_2 NS/SC/AR system was extremely close to the FL spectrum of AChE/MnO_2 NS/SC/AR system (Fig. 2A(b), 2B(b)), the FL intensity of SC and AR did not influence by ATCh or AChE. In the absence of OPs, AChE catalyzed ATCh hydrolysis to produce TCh,

3.3. Characterization of MnO_2 nanosheets

Characterization of the morphology of MnO_2 NS was obtained by transmission electron microscopy. As shown in Fig. 3A, it had a two-dimensional sheet-like morphology. MnO_2 NS have a wide UV

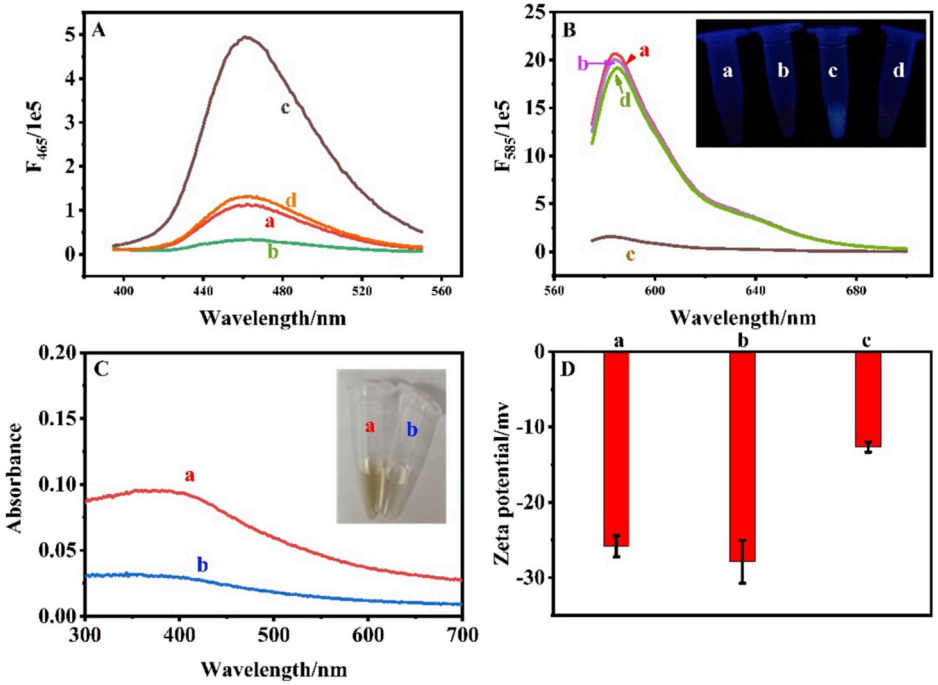

Fig. 2. (A) Fluorescence spectra of SC and (B) Fluorescence spectra of AR. ATCh/MnO2 NS/SC/AR (a), AChE/MnO2 NS/SC/AR (b), ATCh/AChE/MnO2 NS/SC/AR (c), ATCh/AChE/OPs/MnO2 NS/SC/AR (d). (Inset photography of the corresponding fluorescence response under UV light.) (C) UV–vis absorption spectra of MnO2 NS in the (a) absence and (b) presence of AChE. (Inset: the corresponding photos) (D) Zeta-potentials of MnO2 NS (a), Zeta-potentials of MnO2 NS in the (b) absence and (c) presence of AChE.

absorption band ranging from 300 nm to 700 nm and peaks are concentrated at 360 nm (Fig. 3B). Dynamic light scattering data showed that the particle size of MnO_2 NS was ~100 nm (Fig. 3C). All the above characterizations distinctly proved successful synthesis of MnO_2 NS.

3.4. Optimization of reaction conditions

To achieve high sensitivity, some related factors such as the concentrations of the substrate of ATCh, reaction of pH, concentrations of MnO_2 NS, oxidation time of probe pairs were investigated. As the substrate of AChE, ATCh has great influence on producing TCh and consequently affected fluorescence intensity of SC and AR. As shown in Fig. S1A, the biggest fluorescence intensity ratio $(F_{585}/F_{465})/(F_{585}/F_{465})_0$ was observed when the ATCh concentration was 5 mM. $(F_{585}/F_{465})_0$ and (F_{585}/F_{465}) were the fluorescence intensity ratios of the sensor in the absence and presence of AChE respectively. Thus, we fixed the ATCh concentration at 5 mM for the following experiments. pH was an important factor affecting enzyme activity. As shown in Fig. S1B, the ratio of fluorescence intensity increased gradually with the increasing pH, reaching its maximum value at pH 8.5. The ratio decreased slightly with the pH value from 8.5 to 9.0. The enzyme has good catalytic activity in an alkaline environment, however, too high pH also impacts the activity of the enzyme. Thus, we selected 8.5 as the optimal pH for the enzyme reaction. The concentration of MnO_2 NS had a remarkable influence on background signal. As shown in Fig. S1C, 0.5 mg/mL MnO_2 NS was enough to oxidize SC and AR adequately. As shown in Fig. S1D, the FL_{465} values of SC decreased gradually and reached to a plateau at about 30 min. In comparison, the FL_{585} values of AR increased gradually and became level off at about 30 min. Thus, the selected optimal reaction time was 30 min.

3.5. Sensitive detection of AChE

To demonstrate the ability of the proposed strategy to detect OPs sensitively, a range of different concentrations of AChE were measured under optimal conditions. Fig. 4A and Fig. 4B displayed the fluorescent signal of SC and AR corresponding to different contents of AChE. The linear equation was determined to be $F_{465}/F_{585} = 0.0559 + 0.0130$ [AChE] ($R^2 = 0.9908$) (Fig. 4C). The limit of detection (LOD) was calculated to be 1.2 mU/mL. Next, we studied the effects of different concentrations of enzymes on target detection. As shown in Fig. S2, in order to obtain high sensitivity, 50 mU/mL AChE was chosen for OPs detection.

3.6. Sensitive detection of DDVP

To demonstrate the applicability of the developed ratiometric fluorescent sensor for sensitive detection of OPs, DDVP was chosen as a

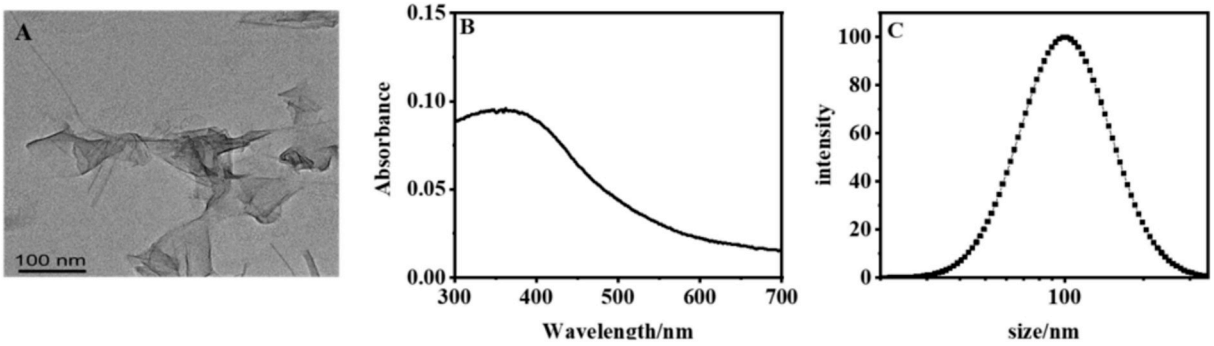

Fig. 3. (A) TEM image of as-synthesized MnO2 NS; (B) UV–vis absorbance spectra of MnO2 NS; (C) DLS characterization of the prepared MnO2 NS.

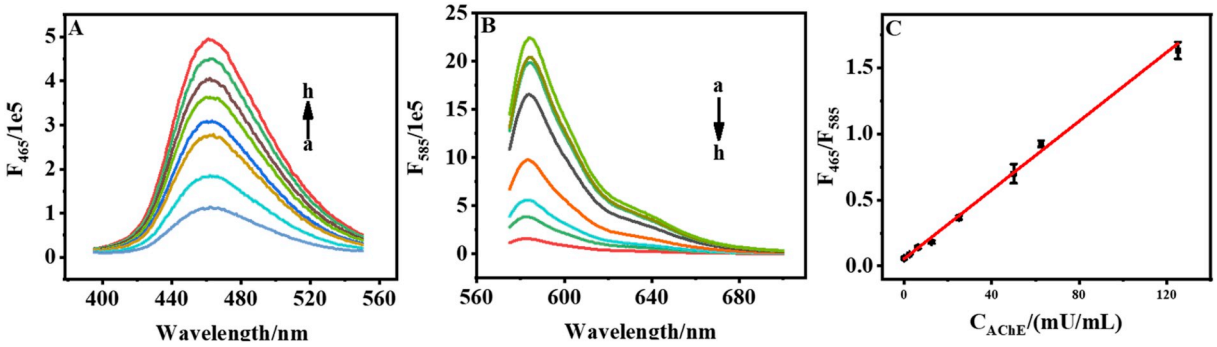

Fig. 4. (A) Fluorescence spectra of the SC in the presence of various concentrations of AChE. (B) Fluorescence spectra of the AR in the presence of various concentrations of AChE: 0, 2.5, 6.25, 12.5, 25, 50, 62.5 and 125 mU/mL (a–h). (C) Linear relationship between F465/F585 versus different concentration of AChE.

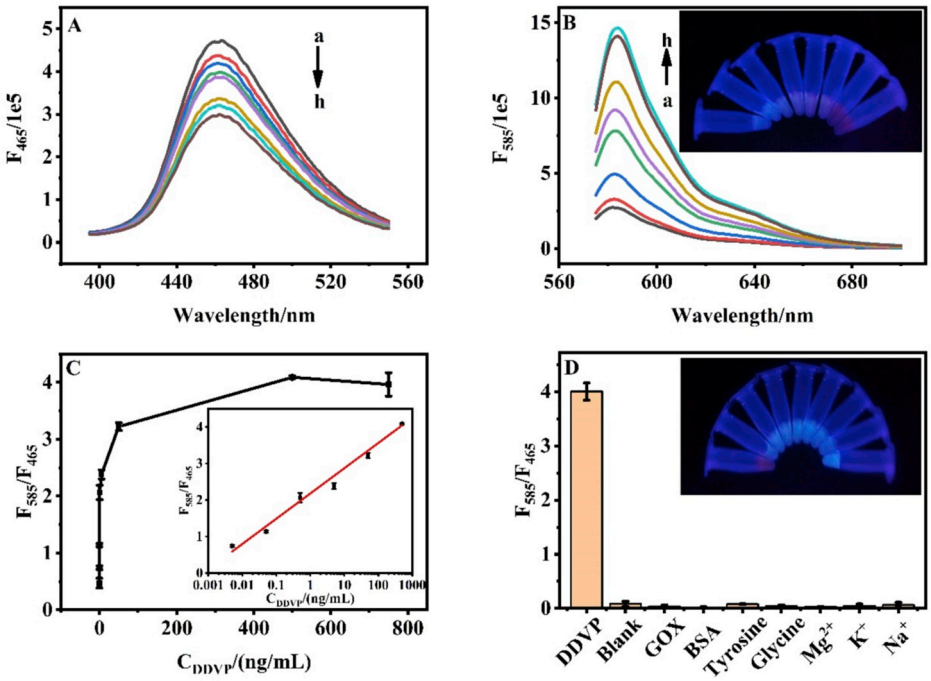

Fig. 5. Fluorescence spectra of the SC (A) and AR (B) in the presence of various concentrations of DDVP. (a) 0, (b) 5 pg/mL, (c) 50 pg/mL (d) 500 pg/mL, (e) 5 ng/mL, (f) 50 ng/mL, (g) 500 ng/mL, (h) 750 ng/mL (Inset: photographs are corresponding to different concentrations of DDVP) (C) Calibration curve of ratiometric fluorescent values (F585/F465) versus different concentrations of DDVP. (Inset: linear relationship between the ratios and logarithmic concentrations of DDVP in the range of 5 pg/mL ~ 500 ng/mL) (D) Selectivity of the ratiometric homogeneous fluorescence sensor for the DDVP against blank assay and other interfering substances. The error bars are obtained via three independent experiments.

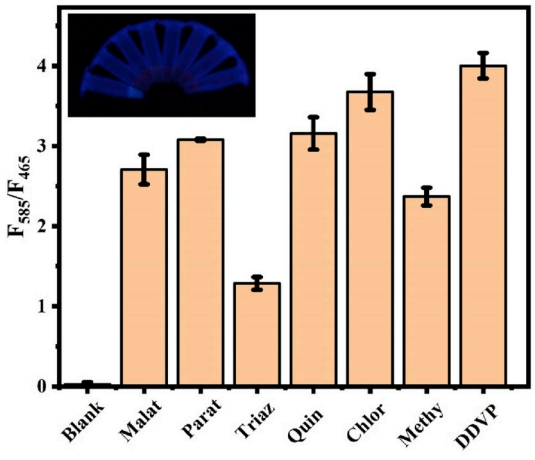

Fig. 6. The comparison of the inhibition effects from other organophosphorus pesticides. The FL intensity ratio (F585/F465) of different types of OPs to ATCh/AChE/SC/AR/MnO2 NS system. Inset shows the color change of corresponding solution with UV irradiation. (For interpretation of the references to color in this figure legend, the reader is referred to the Web version of this article.)

Table 1
Detection DDVP in real lake water samples by the proposed methods.

Sample	Spiked concentration (ng mL^{-1})	Found (ng mL^{-1})	Recovery (%)	RSD (%, n = 3)
1	0.005	0.0053	106.00	8.81
2	0.05	0.0510	102.00	9.29
3	0.5	0.4597	91.94	5.75
4	5	4.6199	92.39	11.02
5	250	246.8607	98.74	11.29

target model. Under optimal conditions, the developed ratiometric fluorescent method was applied for sensing OPs exemplified with different concentrations. As the concentration of OPs increased, the activity of the enzyme was further inhibited, leading to less decomposition of MnO_2 NS and a gradually decrease of SC fluorescence intensity (Fig. 5A). In contrast, the fluorescence intensity of AR was significantly increased (Fig. 5B), which was attributed to the less decomposition of the MnO_2 NS. Simultaneously, as gradually along with the concentration of the OPs increased, the ratio of the fluorescence intensity gradually increased. As illustrated in Fig. 5C, the ratio of fluorescence intensity increased linearly with increment of DDVP concentration from 5.0 pg/mL to 500 ng/mL. A good linear relationship between the ratio

of the fluorescence intensity and logarithm of DDVP concentration was observed (inset). The regression equation for DDVP was described as F_{585}/F_{465} = 2.1807 + 0.6908 log [DDVP] (R^2 = 0.9910), where F_{585}/F_{465} and [DDVP] represented the ratio of the fluorescence intensity and OPs concentration, respectively. The limit of detection was calculated to be 1.6 pg/mL estimated by the 3σ rule, which meant the strategy had a high sensitivity for OPs detection. Under the illumination of the UV lamp, a gradient of color change from blue to red could be seen with the naked eye as a function of concentration. In comparison with most analytical methods (Table S1), the sensitivity of the sensor for OPs detection has been enhanced by 1–3 orders of magnitude.

3.7. Responses of interferences and other OPs

To investigate the selectivity of the strategy, glucose oxidase (GoX), bovine serum albumin (BSA), tyrosine, glycine, Mg^{2+}, K^+ and Na^+ were chosen as interferences. As shown in Fig. 5D, the fluorescence intensity ratio (F_{585}/F_{465}) of sensor for OPs assay was much higher than the interferences (with the concentrations 1000 times higher than OPs), which indicated that the proposed sensor had good selectivity for discriminating of OPs from other interfering substances including biological species and electrolytes owing to the high specific recognition.

This strategy could also be applied for the other OPs detection. Six common pesticides such as malathion, parathion, triazophos, quinalphos, chlorpyrifos and methyl parathion were chosen for detection. It was demonstrated the strategy could also be applied to other OPs detection from the corresponding FL responses (Fig. 6).

3.8. Detection of OPs in water samples

To certify the sensor could be applied to detect practical samples, OPs of various concentrations were added into lake water samples. The results were shown in Table 1. The recoveries of DDVP in lake water were from 91.94% to 106.00%, indicating the method was accurate. The relative standard deviations were from 5.75% to 11.29%. These results showed acceptable recovery rate and relative standard deviation, which suggested the prepared methods possessed good performance for detecting OPs in real water samples.

4. Conclusions

In summary, we designed a ratiometric fluorescent biosensor for sensitive detection of organophosphorus pesticides according to the quenching of SC and the recovery of AR by MnO_2 NS. The sensor relied on the inhibition of enzymaticetching of MnO_2 NS and the fluorogenic substrates of SC and AR assisted ratiometric signal transduction response of MnO_2 NS. Based on the proposed method, quantification of OPs could be achieved downed to 1.6 pg/mL, with a linear range of 5 pg/mL ~500 ng/mL, which is much superior to the OPs biosensor reported previously. The dual signal strategy proposed here can improve the sensitivity of OPs detection. This method provided a new path to construct ratiometric fluorescence biosensors.

Notes

The authors declare no competing financial interest.

CRediT authorship contribution statement

Tiantian Yao: Data curation, Writing - original draft. **Anran Liu:** Formal analysis, Software. **Yong Liu:** Conceptualization, Writing - review & editing. **Min Wei:** Methodology. **Wei Wei:** Funding acquisition, Project administration, Writing - review & editing. **Songqin Liu:** Supervision.

Declaration of competing interest

The authors declare that they have no known competing financial interests or personal relationships that could have appeared to influence the work reported in this paper.

Acknowledgements

We gratefully appreciate the support from The National Key Research and Development Program of China (No, 2018YFC1602800), National Natural Science Foundation of China (21775019), Fundamental Research Funds for the Central Universities and A Project Funded by the Priority Academic Program Development of Jiangsu Higher Education Institutions (Grant Nos. 2242018K3DN04).

Appendix A. Supplementary data

Supplementary data to this article can be found online at https://doi.org/10.1016/j.bios.2019.111705.

References

Aragay, G., Pino, F., Merkoci, A., 2012. Chem. Rev. 112 (10), 5317–5338.
Chen, Y., Tan, C., Zhang, H., Wang, L., 2015. Chem. Soc. Rev. 44 (9), 2681–2701.
Chen, Y., Ye, D., Wu, M., Chen, H., Zhang, L., Shi, J., Wang, L., 2014. Adv. Mater. 26 (41), 7019–7026.
Cheng, N., Song, Y., Fu, Q., Du, D., Luo, Y., Wang, Y., Xu, W., Lin, Y., 2018. Biosens. Bioelectron. 117, 75–83.
Dzudzevic Cancar, H., Soylemez, S., Akpinar, Y., Kesik, M., Goker, S., Gunbas, G., Volkan, M., Toppare, L., 2016. ACS Appl. Mater. Interfaces 8 (12), 8058–8067.
Fan, D., Shang, C., Gu, W., Wang, E., Dong, S., 2017. ACS Appl. Mater. Interfaces 9 (31), 25870–25877.
Fan, H., Zhao, Z., Yan, G., Zhang, X., Yang, C., Meng, H., Chen, Z., Liu, H., Tan, W., 2015. Angew. Chem. Int. Ed. 54 (16), 4801–4805.
Han, T., Wang, G., 2019. J. Mater. Chem. B . 7 (16), 2613–2618.
Hua, X., Yin, W., Shi, H., Li, M., Wang, Y., Wang, H., Ye, Y., Kim, H.J., Gee, S.J., Wang, M., Liu, F., Hammock, B.D., 2014. Anal. Chem. 86 (16), 8441–8447.
Huang, S., Guo, M., Tan, J., Geng, Y., Wu, J., Tang, Y., Su, C., Lin, C.C., Liang, Y., 2018. ACS Appl. Mater. Interfaces 10 (45), 39056–39063.
Kim, K., Tsay, O.G., Atwood, D.A., Churchill, D.G., 2011. Chem. Rev. 111 (9), 5345–5403.
Lee, J., Lee, H.K., 2011. Anal. Chem. 83 (17), 6856–6861.
Li, T., Ackermann, D., Hall, A.M., Famulok, M., 2012. J. Am. Chem. Soc. 134 (7), 3508–3516.
Liu, B., Zeng, F., Wu, S., Wang, J., Tang, F., 2013. Microchim. Acta. 180 (9–10), 845–853.
Liu, G., Guo, W., Yin, Z., 2014. Biosens. Bioelectron. 53, 440–446.
Liu, X., Song, M., Hou, T., Li, F., 2017. ACS Sens. 2 (4), 562–568.
Liu, Y., Lv, B., Liu, A., Liang, G., Yin, L., Pu, Y., Wei, W., Gou, S., Liu, S., 2018. Sens. Actuators B Chem. 265, 675–681.
Lu, L., Su, H., Liu, Q., Li, F., 2018. Anal. Chem. 90 (19), 11716–11722.
Mishra, A., Kumar, J., Melo, J.S., 2017. Biosens. Bioelectron. 87, 332–338.
Ouyang, H., Lu, Q., Wang, W., Song, Y., Tu, X., Zhu, C., Smith, J.N., Du, D., Fu, Z., Lin, Y., 2018. Anal. Chem. 90 (8), 5147–5152.
Qian, G., Wang, L., Wu, Y., Zhang, Q., Sun, Q., Liu, Y., Liu, F., 2009. Food Chem. 117 (2), 364–370.
Sang, Z.Y., Wang, Y.T., Tsoi, Y.K., Leung, K.S., 2013. Food Chem. 136 (2), 710–717.
Tan, M.J., Hong, Z.Y., Chang, M.H., Liu, C.C., Cheng, H.F., Loh, X.J., Chen, C.H., Liao, C.D., Kong, K.V., 2017. Biosens. Bioelectron. 96, 167–172.
Wang, H., Zhang, B., Zhao, F., Zeng, B., 2018. ACS Appl. Mater. Interfaces 10 (41), 35281–35288.
Wang, J., Chow, W., Leung, D., Chang, J., 2012. J. Agric. Food Chem. 60 (49), 12088–12104.
Wang, X., Yu, J., Kang, Q., Shen, D., Li, J., Chen, L., 2016. Biosens. Bioelectron. 77, 624–630.
Wu, X., Song, Y., Yan, X., Zhu, C., Ma, Y., Du, D., Lin, Y., 2017. Biosens. Bioelectron. 94, 292–297.
Yan, X., Li, H., Hu, T., Su, X., 2017a. Biosens. Bioelectron. 91, 232–237.
Yan, X., Song, Y., Wu, X., Zhu, C., Su, X., Du, D., Lin, Y., 2017b. Nanoscale 9 (6), 2317–2323.
Yan, X., Song, Y., Zhu, C., Li, H., Du, D., Su, X., Lin, Y., 2018. Anal. Chem. 90 (4), 2618–2624.
Yan, X., Song, Y., Zhu, C., Song, J., Du, D., Su, X., Lin, Y., 2016. ACS Appl. Mater. Interfaces 8 (34), 21990–21996.
Yang, Z.R., Wang, M.M., Wang, X.S., Yin, X.B., 2017. Anal. Chem. 89 (3), 1930–1936.
Zhao, F., Yao, Y., Li, X., Lan, L., Jiang, C., Ping, J., 2018. Anal. Chem. 90 (19), 11658–11664.
Zhao, Z., Fan, H., Zhou, G., Bai, H., Liang, H., Wang, R., Zhang, X., Tan, W., 2014. J. Am. Chem. Soc. 136 (32), 11220–11223.